01 Jan 1988

Argon Metastable-cadmium Dihalide Energy Transfer Collisions In A Flowing Afterglow

Christopher L. Bohler

Laird D. Schearer
Missouri University of Science and Technology

Recommended Citation

C. L. Bohler and L. D. Schearer, "Argon Metastable-cadmium Dihalide Energy Transfer Collisions In A Flowing Afterglow," *The Journal of Chemical Physics*, vol. 89, no. 4, pp. 1950 - 1957, American Institute of Physics, Jan 1988.
The definitive version is available at https://doi.org/10.1063/1.455093

RESEARCH ARTICLE | AUGUST 15 1988

Argon metastable–cadmium dihalide energy transfer collisions in a flowing afterglow

Christopher L. Bohler; Laird D. Schearer

J. Chem. Phys. 89, 1950–1957 (1988)
https://doi.org/10.1063/1.455093

Argon metastable–cadmium dihalide energy transfer collisions in a flowing afterglow

Christopher L. Bohler[a] and Laird D. Schearer
Department of Physics, University of Missouri at Rolla, Rolla, Missouri 65401

(Received 21 January 1988; accepted 12 May 1988)

The energy dependence of dissociating collisions between argon metastable atoms and cadmium dihalide molecules have been studied in a flowing afterglow apparatus. The fluorescence spectra obtained in the range of 3000–7600 Å which result from the $Ar(^3P_2) + CdX_2$ interactions indicate a dominant dissociative excitation production mechanism. The emission spectra are used to narrow the uncertainty in the currently accepted values for the dissociation energy of the CdX_2 molecules. The Wigner spin rule (conservation of total electronic spin) was verified for these processes as shown by the dominance of final state triplet production as compared to the virtual absence of singlet spin state production.

I. INTRODUCTION

A long term project in this laboratory has been the study of the collision dynamics and spin dependence of thermal energy transfer collisions. These collisions have been investigated for many years and manifest themselves in a number of excitation channels. One such interaction which is of interest here is dissociative excitation in which

$$X^* + AB \rightarrow X + (AB)^*$$

followed by

$$(AB)^* \rightarrow A + B^*,$$

where X^* is an incident metastable atom with an internal energy comparable to or greater than the combined dissociation and excitation energy of the complex AB.

We have chosen to use the flowing afterglow method for this study because in those cases where the effect of multiple collisions can be ignored (or at least accounted for) the flowing afterglow apparatus provides ease of use in addition to substantial increases in the number of interactions per unit time. This follows largely from the much greater densities of participants which are available in the flowing afterglow. The flowing afterglow, data acquisition system, and flowing afterglow diagnostics are discussed in Secs. II A–II C, respectively.

The original stimulus for these particular studies was provided by the report of an increased lasing efficiency on the mercuric bromide HgBr(B–X) transition due to the addition of small amounts of N_2 into an $HgBr_2$ plasma.[1] Performing the first of many such experiments in this laboratory, Fahey *et al.*[2] were able to show in a molecular beam environment that the increase in efficiency was due to the direct pumping of the HgBr upper laser level via dissociative excitation of $HgBr_2$ by vibrationally excited N_2 molecules in the $A\,^3\Sigma_u^+$ metastable state. In addition, with the discovery of several new molecular lasers utilizing metal–halogen molecules, renewed interest was generated in energy transfer collisions which resulted in dissociative excitation of the molecular system.[3]

Although interactions with mercuric dihalide molecules have been studied extensively,[4] only photodissociative excitation experiments have been performed on the cadmium dihalide species.[3,5] This is due to the strong absorption exhibited by CdX_2 in the UV region and the use of excimer lasers as laser pump sources. The X indicates the halogen atom I, Br, or Cl.

In Sec. III experimental fluorescence data are presented and the energy dependence is discussed. With respect to the dissociation mechanism, effects of total electron spin conservation (according to the Wigner spin rule[6]) have been observed in a number of molecular systems.[7,8] Similar effects for the argon metastable–cadmium dihalide systems have been observed and will be discussed in this section as well.

II. EXPERIMENTAL APPARATUS

A. Flowing afterglow

Our fast flowing afterglow is modeled after that of Schmeltekopf and Broida[9] and is shown in Fig. 1. The basic apparatus consists of a microwave discharge, a 25 cm diameter pyrex cylinder which encloses the interaction region, a quartz window for viewing the emitted fluorescence, an oven, and a Roots pump.

The standard purity noble gas to be excited enters through a converging–diverging pyrex nozzle located just below an Evenson-type microwave cavity. The discharge struck in the cavity is separated from the center of the interaction region by 12 cm. The center of the interaction region is defined by the placement of an oven which contains the target species in powder form. The oven consists of a quartz ampoule which is wrapped with Nichrome wire. Although no attempt has been made to determine the oven temperature directly, the oven current is varied between 2.5 and 3.5 A depending upon the vapor pressure of the molecular constituent which is being introduced. In the case of the cadmium containing compounds which we are studying, the vapor pressure at a fixed temperature increases with the Z of the halogen molecular constituent.

In order to maintain a steady flow in the afterglow system, a high throughput Roots pump is connected to the apparatus through a 10 cm diam copper tube. The flow rate at

[a] Permanent address: Texas Instruments, P. O. Box 660246, M/S 8276, Dallas, TX 75266.

 0021-9606/88/161950-08$02.10

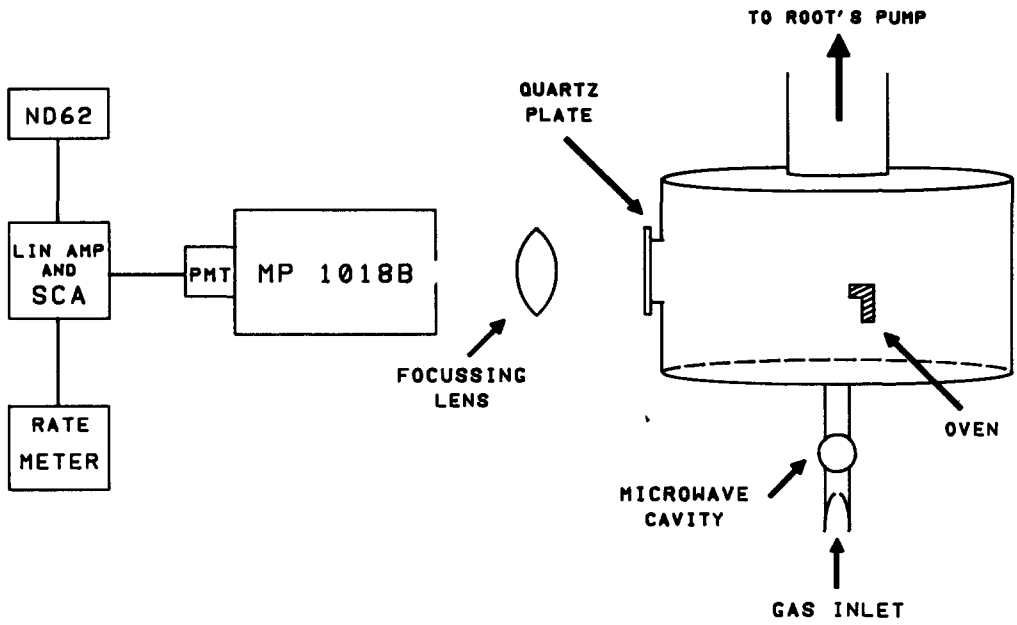

FIG. 1. Flowing afterglow apparatus. The apparatus consists of a gas inlet region, a microwave excitation region, an oven to introduce the target gas, and a Root's pump to maintain a steady flow rate.The data collection system consists of a monochromator, photomultiplier tube (PMT), linear amplifier (LIN AMP), single channel analyzer (SCA), rate meter, multichannel analyzer (ND 62), and IBM PC (not shown). The focusing lens is the link between the afterglow and the data acquisition system.

the throat of the pump is 516 ft^3/min and, as a result, the velocity of the noble gas in the interaction region is approximately 10^3–10^4 cm/s. The pressure in the pyrex cylinder is monitored with a thermocouple gauge, and, although not very accurate, it is useful for reproducing conditions from one day to the next. Typical afterglow pressures range from 0.03 to 1.0 Torr.

B. Data acquisition system

The emitted radiation is collected with a lens which is focused onto the slits of a 1/2 m MP1018B Pacific Scanning Monochromator. A Hamamatsu R928 photomultiplier tube (PMT) with a response range from 185.0 to 900.0 nm is mounted at the exit slits of the monochromator and is contained in a thermoelectrically cooled housing. The PMT is typically cooled to -20 °C which reduces the dark current from 10 nA at room temperature to about 10^{-2} nA. The signal from the PMT is sent through a linear amplifier (LIN AMP) and single channel analyzer (SCA) to a ratemeter and Nuclear Data ND62 multichannel analyzer (MCA). The ND62 is set in the photon counting mode and is interfaced to an IBM PC for data storage.

The scanning monochromator and ND62 MCA are synchronized so that an appreciable amount of the response range of the detector may be monitored in a single run. However, conditions are such that all transitions in the fluorescence spectrum are easily resolved. Typical experimental parameters are 0.3 ms dwell time per channel for the 2048 channel MCA, a scan rate of 500 Å/min for the monochromator, and slit widths at the entrance and exit ports of the monochromator of 75 microns.

These conditions are such that a typical run covers a wavelength range from approximately 3000 to 7600 Å. At about 5500 Å a Hoya Y48 cutoff filter is inserted in front of the entrance slits of the monochromator. As a result, second order effects are not observed beyond this point. In addition, for the entire wavelength region which is scanned subsequent to the insertion of the filter, the Y48 has a flat transmission coefficient of 91%. This must be taken into account when correcting for the wavelength response of the acquisition system.

The ND62 employs an autosequencing mode such that a minimal amount of operator participation is required from the time that the run begins to the time that the data is stored on the PC.

C. Flowing afterglow diagnostics

Since our studies involve energy transfer from the noble gas metastable state, we would like to optimize the metastable density in the interaction region while minimizing the effects due to the other constituents produced in the discharge. For example, typical densities of the various constituents in our argon afterglow are $Ar(^3P_2)$:5×10^9 cm^{-3}, $Ar(1\,^1S_0)$:10^{16} cm^{-3}, and Ar^+ and e^-:5×10^8 cm^{-3} in the interaction region. Although other species such as Ar_2^m and Ar_2^+ may be present in the afterglow, their effects are not significant at our lower operating pressures.

We may further investigate the dependence of the argon metastable density on various afterglow conditions by monitoring the line absorption of the metastable resonance radiation emitted from a noble gas discharge lamp as it traverses the interaction region. For argon the metastable resonance transition occurs at 811.5 nm ($1s_5$–$2p_9$:$^3P_2$–$^3D_3$).

In order to calculate the metastable density absolutely, the fractional absorption and path length traversed must be determined.[10] Results for the metastable density as a function of afterglow pressure are shown in Fig. 2 for argon. These data were taken at a microwave discharge power of 0.5 W. The oscillator strength used was $f=0.509$ for $Ar(^3P_2$–$^3D_3)$.[11]

The values obtained for the densities are only reliable to approximately $\pm$ 50% due to the inaccuracy in determining the path length. The recombination light in the pyrex cylinder was used as a visual guide to determine the path length.

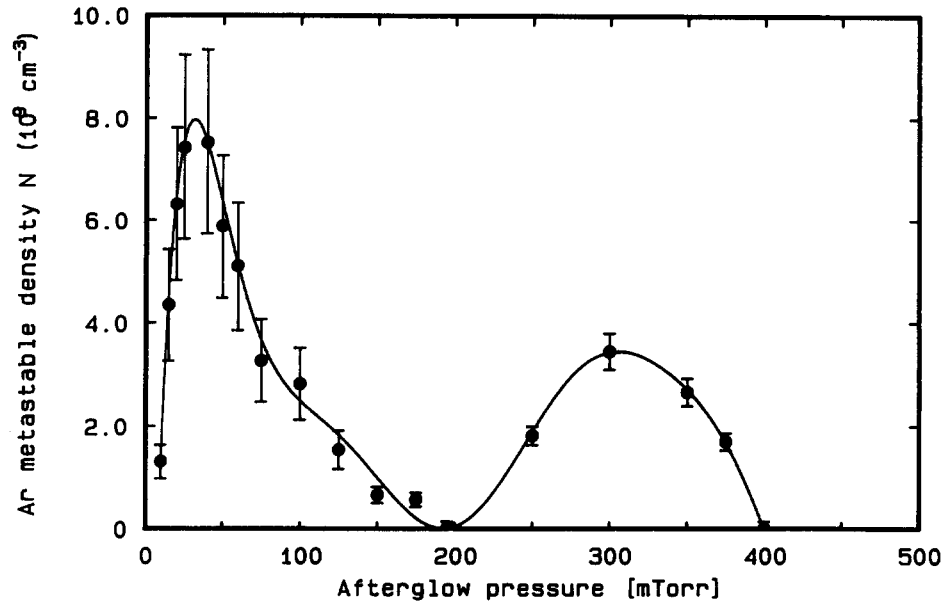

FIG. 2. Ar($^3P_2$) density vs afterglow pressure at a microwave power of 0.5 W.

At the lower pressures the path length was not easily determined because a well-defined absorption region was not readily observable. A peak density of 8×10^9 cm^{-3} is obtained at about 30 mTorr afterglow pressure. The reason for the minimum at approximately 200 mTorr is inconclusive although it appears as if it may be associated with the onset of turbulence in the afterglow region as diamond-shaped shock waves are observed.

The Ar($^3P_0$) density was also determined by monitoring the line absorption due to the $3p^5 4s'[1/2]_0(^3P_0)\rightarrow 3p^5 4p'[3/2]_1$ transition at 794.8 nm. The $^3P_0$ density maintained the same shape as the $^3P_2$ density; however, its amplitude was at least an order of magnitude smaller throughout the pressure regime.

It was observed that the metastable argon population decreased as the discharge power was increased. This is caused by metastable interactions with hot electrons in the discharge region. Thus, much care was taken to run at the lowest microwave power possible while still maintaining a steady discharge. The argon metastable density was maximized for the data to be presented.

In order to make any conclusive statements about the data, the data acquisition system had to be corrected for response efficiency as a function of wavelength. A relative calibration was performed by placing a 200 W quartz iodine tungsten-filament lament lamp at the center of the interaction region and comparing the signal strengths obtained to the NBS standard of spectral irradiance.[12]

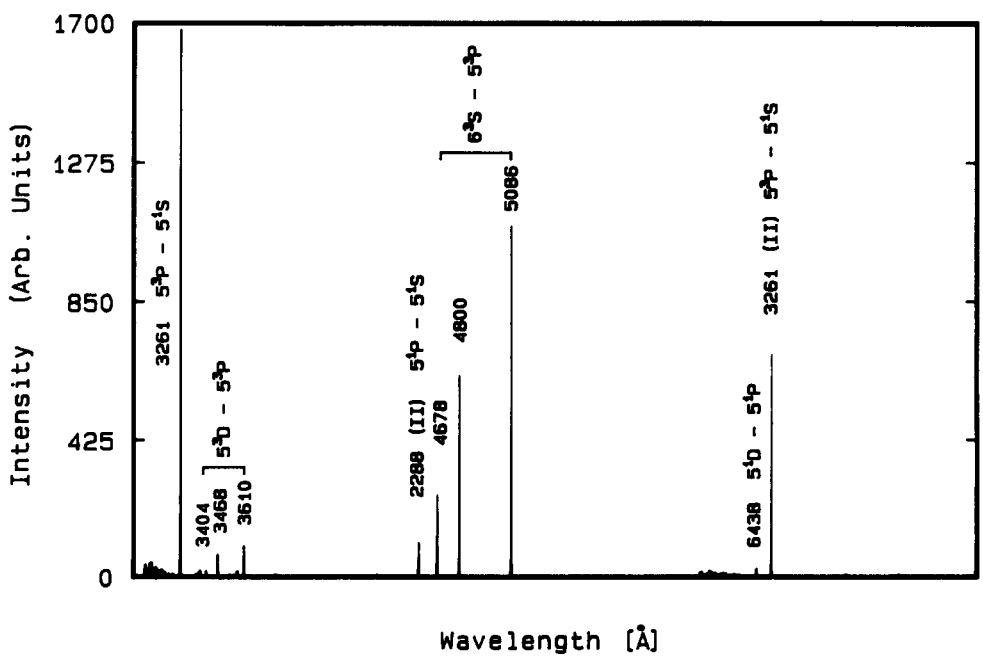

FIG. 3. $Ar''' + CdI_2$ fluorescence spectrum from 3000–7600 Å. Data taken at an afterglow pressure of 30 mTorr and is uncorrected for frequency response of the data acquisition system. (II) indicates second order.

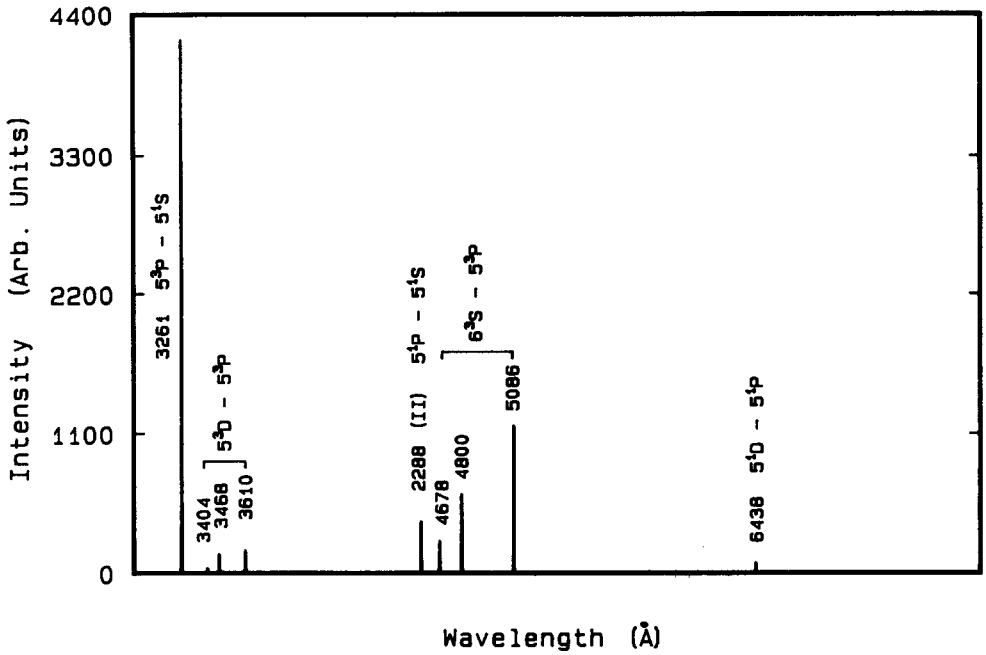

FIG. 4. $Ar^m + CdI_2$ fluorescence spectrum from 3000–7600 Å. The data has been obtained at an afterglow pressure of 30 mTorr and has been corrected for frequency response as well as background subtracted. (II) indicates second order.

III. OPTICAL SPECTROSCOPIC RESULTS

A number of excitation mechanisms have been observed for various excited atom collisions with metal halide molecules:

$$A^* + MX_2 \rightarrow A + MX^* + X, \quad (1)$$

$$A^* + MX_2 \rightarrow A + MX + X^*, \quad (2)$$

$$A^* + MX_2 \rightarrow A + M^* + X + X, \quad (3)$$

where A^* is the incident excited atom, M is the Group IIB metal atom, and X_2 is the dihalide species. The excitation mechanism is determined by the available energy of the incident atom, as well as the curve crossings of the entrance and exit potential surfaces.

The fluorescence spectrum obtained as a result of quenching of the argon metastable atomic state by, CdI_2 is shown in Fig. 3. The data was taken at optimum metastable production conditions (i.e., 0.5 W microwave power and 30 mTorr afterglow pressure). Special care was taken to ensure operation in the linear response region of the data acquisition system.

By referring to the figure, one finds that the wavelength ranges from 3000–7600 Å for this run. Other than a small background signal which results from a water vapor impuri-

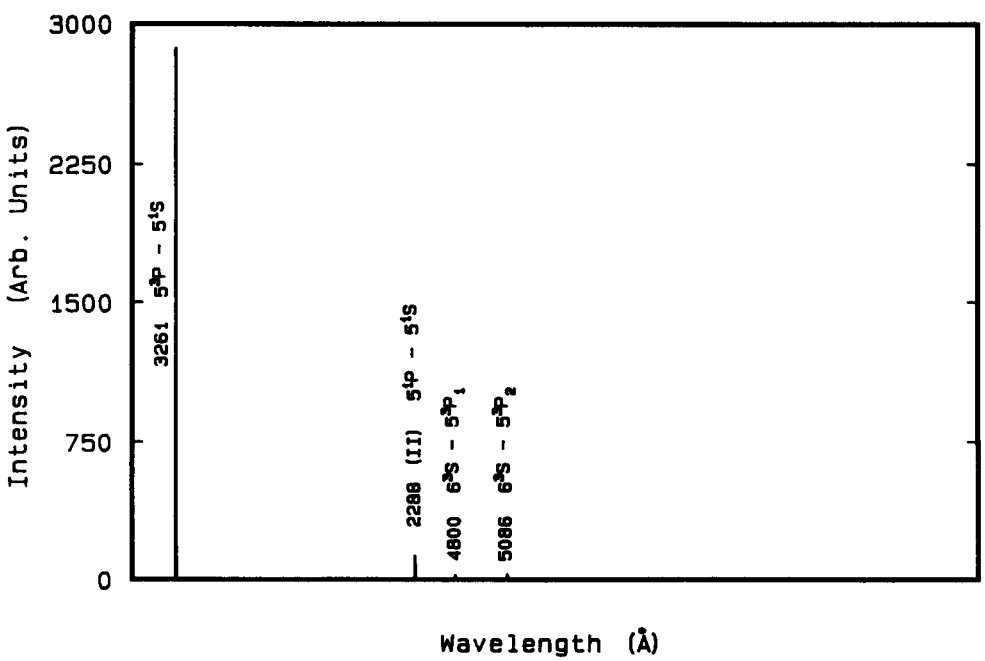

FIG. 5. $Ar^m + CdBr_2$ fluorescence spectrum from 3000–7600 Å. The data has been obtained at an afterglow pressure of 30 mTorr and has been corrected for frequency response as well as background subtracted. (II) indicates second order.

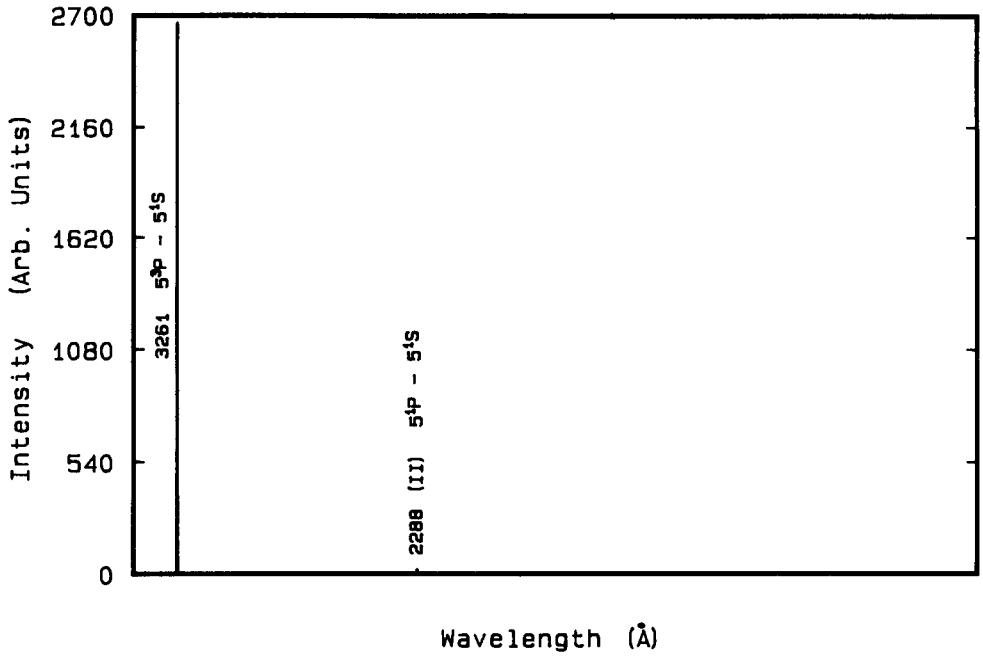

FIG. 6. $Ar^m + CdCl_2$ fluorescence spectrum from 3000–7600 Å. The data has been obtained at an afterglow pressure of 30 mTorr and has been corrected for frequency response as well as background subtracted. (II) indicates second order.

ty (at approximately 3100 Å and also appearing in second order), only fluorescence from neutrally excited cadmium states is observed. This is indicative of a dissociative excitation process [Eq. (3) in the processes listed above] in which the metastable atom gives up its energy (11.55 eV) to dissociate the molecule as well as excite the cadmium atom into a higher lying neutral state:

$$Ar(^3P_2) + CdX_2(^1\Sigma) \rightarrow Ar(^1S_0) + Cd^* + X(^2P) + X(^2P),$$

where X indicates the halogen atom I, Br, or Cl.

However, no quantitative statements can be made as to the production efficiencies of the various populated states unless the data is corrected for the frequency response of the data acquisition system. Thus, Fig. 4 shows the $Ar(^3P_2) + CdI_2$ fluorescence data after it has been background subtracted and corrected for the detection apparatus response efficiency. The comparable fluorescence spectra for the $CdBr_2$ and $CdCl_2$ molecular systems are shown in Figs. 5 and 6, respectively. Also, Table I shows the relative corrected fluorescence intensities which result from the dissociative excitation process in each of the three cadmium halide species being studied. There are some interesting characteristics to be noted for the $Ar^m + CdX_2$ data:

(1) The spin forbidden intercombination transition in cadmium (5^3P–$5\,^1S$) at 3261 Å is the dominant line in the spectrum.

(2) The cadmium resonance transition ($5\,^1P$–$5\,^1S$) which one might expect to be the strongest line is less than 8% as intense as the intercombination light for each of the cadmium halides being studied.

(3) The quenching of the $Ar(^3P_2)$ atoms appear to lead, on the whole, to a much greater production efficiency of the cadmium triplet levels as compared to the singlet states.

(4) No cadmium levels lying above the $5\,^3D$ state at 7.37 eV are populated in the energy transfer collisions.

These statements are further exemplified by comparing the fluorescence spectrum to that obtained from a typical cadmium discharge lamp.[13] In Fig. 7 the relevant neutral lines of cadmium which are produced in the discharge are shown. Again, the significant points may be enumerated:

(1) The $5\,^1P$–$5\,^1S$ resonance transition is the most intense line in the spectrum and is 50 times that of the intercombination line. Since both the $5\,^1P$ and $5\,^3P$ states are easily accessible in the dissociative excitation process (as will be shown), these data certainly support our claim that there is a spin dependence involved in the dissociation mechanism.

(2) The appearance of emission from the discharge at 325.3 and 308.1 nm which results from a $Cd(7\,^3S)$ population, together with the absence of such emission in the afterglow fluorescence points to a truncation in the $Ar^m + CdI_2$

TABLE I. Corrected relative fluorescence intensities obtained from $Ar^m + CdX_2$ optical spectra.

Transition	$Ar^m + CdX_2$ wavelength (nm)	Relative intensity CdI_2	$CdBr_2$	$CdCl_2$
$Cd^+(5\,^2D_{5/2}$–$5\,^2P_{3/2})$	325.1	...	...	...
$Cd(5\,^3P_1$–$5\,^1S_0)$	325.9	4805	4608	3013
$Cd(5\,^3D$–$5\,^3P)$	340.4	41	...	...
$Cd(5\,^3D$–$5\,^3P)$	346.6	176	...	...
$Cd(5\,^3D$–$5\,^3P)$	361.0	230	...	...
$Cd^+(5\,^2D_{3/2}$–$5\,^2P_{1/2})$	441.6	...	...	...
$Cd(5\,^1P$–$5\,^1S_0)$	457.6 (II)	410	141	31
$Cd(6\,^3S_1$–$5\,^3P_0)$	467.8	290	...	...
$Cd(6\,^3S_1$–$5\,^3P_1)$	480.0	836	28	...
$Cd(6\,^3S_1$–$5\,^3P_2)$	508.6	1241	39	...
$Cd(5\,^1D$–$5\,^1P)$	644.0	120	...	...

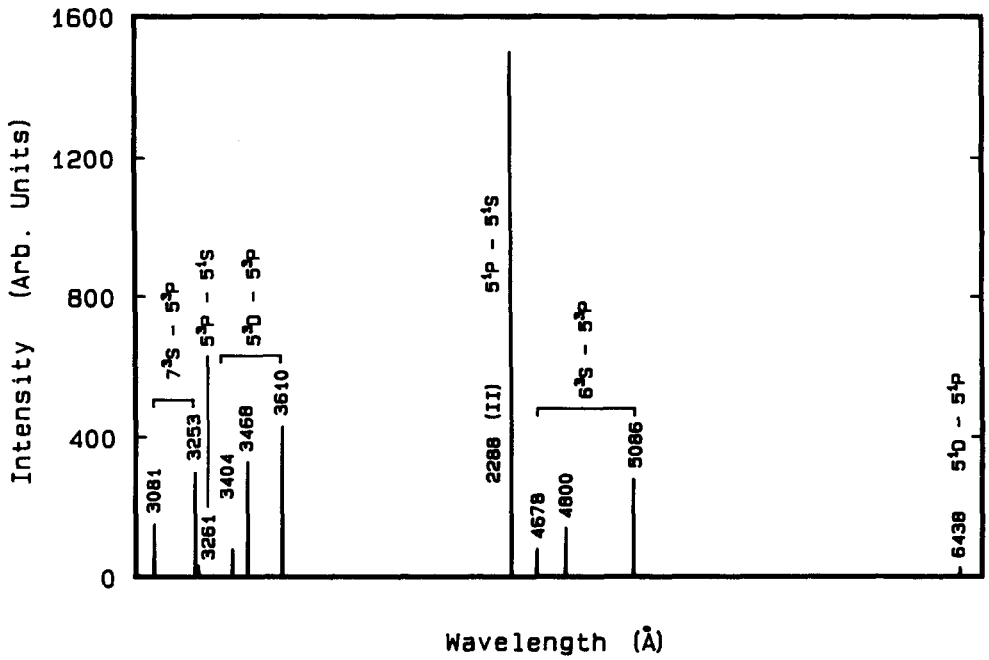

FIG. 7. Cadmium arc lamp neutral fluorescence spectrum from 3000–6500 Å. Obtained from Ref. 17. (II) indicates second order.

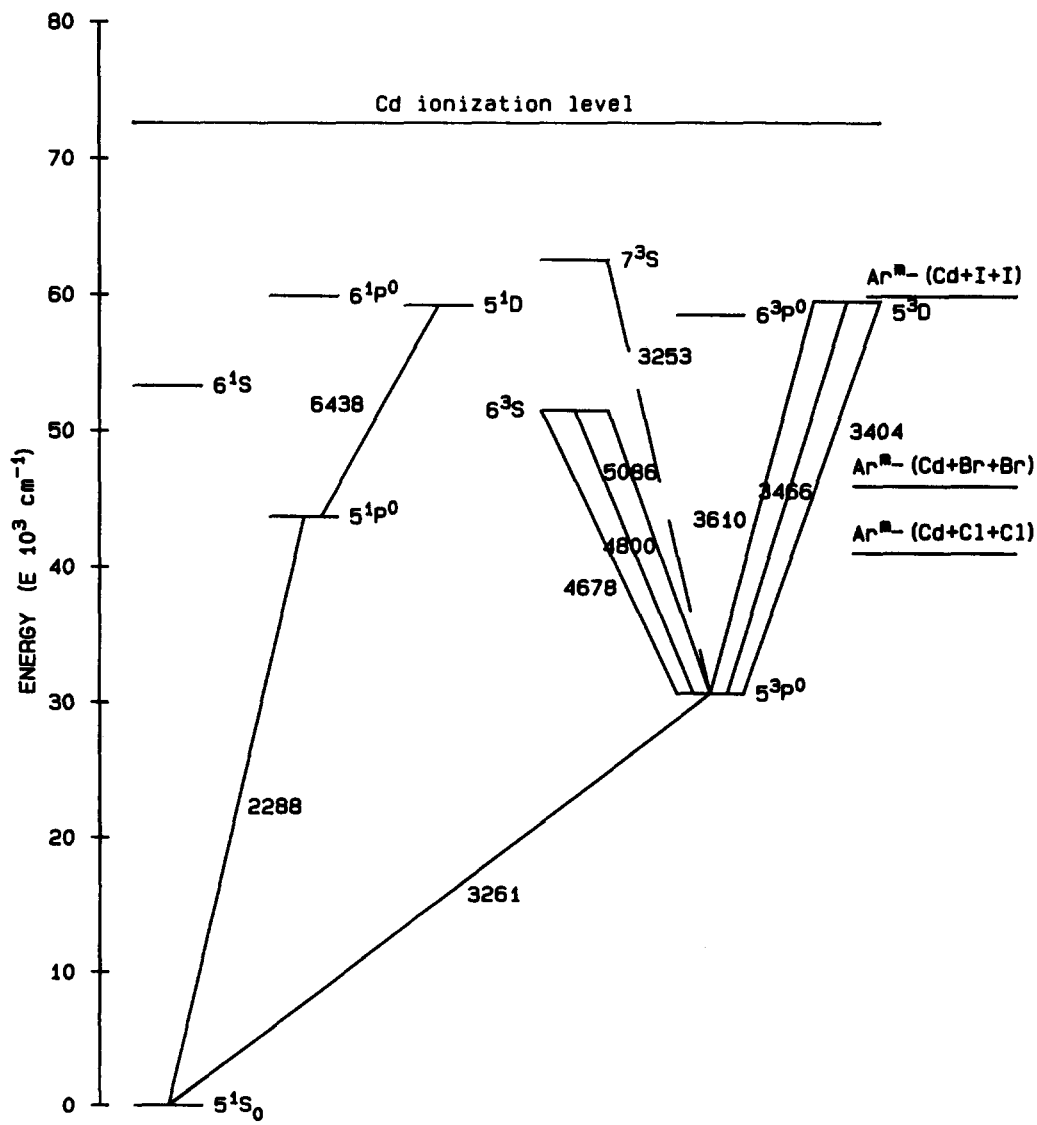

FIG. 8. Cadmium energy level diagram and relevant transitions. The excitation energy available for each of the cadmium halide systems is shown on the right-hand side.

fluorescence spectrum. This truncation will be used to determine the excitation channels by which the dissociation mechanism proceeds. In addition, since the dissociation energies of the cadmium halogen molecules are only known to about 36%,[14] we can use the absence of certain emission lines to determine a narrower uncertainty range in the dissociation energies of these molecules.

The fact that there is a preferential population of the triplet electronic levels in the neutral final states of cadmium support the validity of the Wigner spin rule, since in this case both the precollision and postcollision systems can be formed in a combined triplet spin state. Such "propensity rules" involving spin conservation in similar systems have previously been reported in the literature.[15] In addition, on the basis of the discussion to follow, a final state in which the halogen atoms take up the spin of the parent system is energetically inaccessible. The energy dependence of the optical spectrum obtained for the CdX_2 system may be explained in the following manner:

The initial assumption for our model is that as a result of the collision between the metastable atom and the molecule, the CdI_2 is dissociated so as to produce three atomic constituents in the final state. The precollision system contains 93 144 cm^{-1} of internal energy in the $Ar(^3P_2)$ state while the energy required to dissociate the molecule (i.e., $CdI_2 \rightarrow Cd + I + I$) lies between 27 281 and 39 173 cm^{-1}. Thus, there is a 36% uncertainty in the dissociation energy of the CdI_2 molecular system. Therefore, the excess energy that is available to excite the atomic constituents is such that $53\,971 \leqslant E \leqslant 65\,863$ cm^{-1}. Using the same simple model in the cases of $CdBr_2$ and $CdCl_2$ allow the excitation energies to be determined as $42\,430 \leqslant E \leqslant 49\,426$ cm^{-1} and $34\,705 \leqslant E \leqslant 47\,297$ cm^{-1}, respectively. In Fig. 8 the midpoints of these ranges are compared to the relevant cadmium energy levels and associated transitions (wavelengths in Å) in order to identify the states that are energetically accessible. The excitation energies are shown on the right. The indication is that, for the CdI_2 system, any level lying below the $Cd(5\,^3D)$ state is energetically accessible. However, if the uncertainty in the dissociation energy is taken into account, levels up to $Cd(7\,^1P)$ become accessible. Similar arguments are invoked for the $CdBr_2$ and $CdCl_2$ molecules. Thus, the truncations of the emission spectra allow the determination of upper bounds for the dissociation energies for each of the cadmium dihalide species being studied. Unfortunately, using this particular method does not distinguish a lower bound as any one of the lower lying levels may be populated in the process.

Thus, the upper bound determined for each of the cadmium halide species is shown in Table II and is compared to results found in the literature.[14] Note that for CdI_2 and $CdCl_2$ there is indeed an improvement in the current values; however, for $CdBr_2$ no additional information has been gained.

The model for dissociation discussed previously also suggests that for the CdI_2 system only transitions from excited states lying at or below the $Cd(5\,^3D)$ level should be observed. The same conditions apply to the $Cd(5\,^1P)$ and $Cd(5\,^3P)$ levels for $CdBr_2$ and $CdCl_2$, respectively. Referring to Figs. 4–6, we find that the predictions are valid for the states that are significantly populated. The very greatly reduced fluorescence intensities which originate from levels not predicted to be populated result from the small $Ar(^3P_0)$ metastable density which lies about 0.2 eV higher in energy than the $Ar(^3P_2)$ atoms.

TABLE II. Comparison of upper bounds for cadmium dihalide dissociation energies. Values from the literature are shown in column two. Values obtained from fluorescence spectra are shown in column three.

Target gas	Upper bound for dissociation energy[a] (cm^{-1})	Upper bound for dissociation energy[b] (cm^{-1})
CdI_2	39 173	35 873
$CdBr_2$	50 714	52 772
$CdCl_2$	58 409	54 804

[a] Reference 14.
[b] This work.

Thus, our model is successful in describing on an energy basis the dissociation process between the argon metastable atoms and the cadmium dihalide species. This confirms the validity of the initial assumption that the molecule was segregated into three independent atoms as a result of the collision. If this were not the case then the other mechanisms stated earlier would be invoked. If the channel is considered in which $CdX_2 \rightarrow Cd^* + X_2$, the excess energy available for excitation of the final state products would now be increased by an amount equal to the binding energy of the dihalide molecule. Since this binding energy is in the range of 1.5–2.0 eV, one would expect to see populations of the energy levels well above those that are observed. These observations are perfectly consistent with the fact that CdX_2 is a linear triatomic molecule in the ground state. One would not expect the iodine atoms to recombine after the collision has occurred because of the linear configuration in which the iodine atoms are separated by the cadmium atom.

On the other hand, the reaction channel $CdX_2 \rightarrow CdX^* + X$ would result in the observation of molecular transitions within the response range of our data acquisition system. Molecular bands corresponding to these CdX^* states do not appear in our spectra.

IV. CONCLUSIONS

The energy dependence of energy transfer collisions between argon metastable atoms and cadmium dihalide molecules have been studied in a flowing afterglow apparatus. By monitoring the fluorescence that is emitted as a result of the interaction, the following conclusions can be made:

(1) In the region of the spectrum observed (2000–9000 Å), neutrally excited cadmium is produced as a result of the dissociation of the linear triatomic cadmium halogen molecule by the incident metastable atom.

(2) The truncation of the fluorescence spectra is used to better determine the dissociation energies of the cadmium dihalide species.

(3) The Wigner spin rule is a very important feature in determining which final states are populated.

[1]R. Burnham, Appl. Phys. Lett. **33**, 156 (1978).
[2]D. W. Fahey and L. D. Schearer, J. Chem. Phys. **72**, 6318 (1980).
[3]J. Maya, IEEE J. Quantum Electron. **15**, 579 (1979); M. Kawasaki, S. J. Lee, and R. Bersohn, J. Chem. Phys. **71**, 1235 (1979); E. Gerck and E. Fill, IEEE J. Quantum Electron. **17**, 2140 (1981).
[4]T. D. Dreiling and D. W. Setser, Chem. Phys. Lett. **74**, 211 (1980); T. D. Dreiling, D. W. Setser, and S. Ferrero, J. Chem. Soc. Faraday Trans. 2 **78**, 1311 (1982).
[5]S. G. Dinev, H.-U. Daniel, and H. Walther, Opt. Commun. **41**, 117 (1982).
[6]E. Wigner, Nachr. Akad. Wiss. Gottingen, Math-Phys. Chem. 375 (1927).
[7]E. S. Fishburne, Grumman Research Department Report No. RE-3465 (1968); L. D. Schearer, J. Chem. Phys. **84**, 1408 (1986).
[8]E. L. Milne, J. Chem. Phys. **52**, 5360 (1970); I. Nadler and S. Rosenwaks, Chem. Phys. Lett. **69**, 266 (1980).
[9]A. C. Schmeltekopf and H. P. Broida, J. Chem. Phys. **39**, 1261 (1963).
[10]A. C. G. Mitchell and M. W. Zemansky, *Resonance Radiation and Excited Atoms* (Cambridge University, Cambridge, 1961), pp. 120 and 323.
[11]A. Kono and S. Hattori, Phys. Rev. A **29**, 2981 (1984).
[12]R. Stair, W. E. Schneider, and J. K. Jackson, Appl. Opt. **2**, 1151 (1963).
[13]A. N. Zaidel', V. K. Prokof'ev, S. M. Raiskii, V. A. Slavnyi, and E. Ya. Schreider, *Tables of Spectral Lines* (Plenum, New York, 1970).
[14]V. I. Vedenyev, L. V. Gurvich, V. N. Kondrat'yev, V. A. Medvedev, and Ye. L. Frankevich, *Bond Energies, Ionization Potentials, and Electron Affinities* (Arnold, London, 1966).
[15]C. J. Duthler and H. P. Broida, J. Chem. Phys. **59**, 167 (1973); W. Lee and R. M. Martin, *ibid.* **64**, 678 (1976); and L. D. Schearer, *ibid.* **84**, 1408 (1986).